



CHORUS

This is the accepted manuscript made available via CHORUS. The article has been published as:

Understanding Signatures of Emergent Magnetism in Topological Insulator/Ferrite Bilayers

Lauren J. Riddiford, Alexander J. Grutter, Timothy Pillsbury, Max Stanley, Danielle Reifsnyder Hickey, Peng Li, Nasim Alem, Nitin Samarth, and Yuri Suzuki

Phys. Rev. Lett. **128**, 126802 — Published 24 March 2022

DOI: [10.1103/PhysRevLett.128.126802](https://doi.org/10.1103/PhysRevLett.128.126802)

Understanding Signatures of Emergent Magnetism in Topological Insulator/Ferrite Bilayers

Lauren Riddiford,^{1,2,*} Alexander Grutter,³ Timothy Pillsbury,⁴ Max Stanley,⁴ Danielle Reifsnnyder Hickey,⁵ Peng Li,⁶ Nasim Alem,⁵ Nitin Samarth,⁴ and Yuri Suzuki^{1,2}

¹*Department of Applied Physics, Stanford University*

²*Geballe Laboratory for Advanced Materials*

³*National Institute of Standards and Technology*

⁴*Department of Physics, Pennsylvania State University*

⁵*Department of Materials Science, Pennsylvania State University*

⁶*Department of Electrical Engineering and Computer Science, Auburn University*

(Dated: February 24, 2022)

Magnetic insulator/topological insulator heterostructures have been studied in search of chiral edge states via proximity induced magnetism in the topological insulator, but these states have been elusive. We identified $\text{MgAl}_{0.5}\text{Fe}_{1.5}\text{O}_4/\text{Bi}_2\text{Se}_3$ bilayers for a possible magnetic proximity effect. Electrical transport and polarized neutron reflectometry suggest a proximity effect, but structural data indicate a disordered interface as the origin of the magnetic response. Our results provide a strategy via correlation of microstructure with magnetic data to confirm a magnetic proximity effect.

The emergence of magnetism via a proximity effect has been exploited in many low dimensional materials, including ultra-thin film and 2D materials. By doing so, one can realize magnetic properties in these materials not observed in the bulk nor achievable via doping or functionalization. Magnetic proximity effects (MPEs) have been studied in magnetic heterostructures for many applications including spintronics [1], valleytronics [2], and topological phenomena [3]. Crucial to the observation of a theoretically predicted MPE is an abrupt interface with little to no interdiffusion or interface roughness. Non-idealities at the interface can give rise to behaviors that appear to be a MPE [4].

There is significant interest in realizing magnetic topological insulators (TIs) at elevated temperatures by MPE with a known ferromagnet since bulk magnetic TI phases have thus far been limited to low temperatures. Topological insulators are characterized by conduction along non-dissipative helical edge states (or surface states in the case of 3D TIs) while the bulk of the material is insulating [5]. By making TIs magnetic, these helical edge states are transformed to chiral edge states as time-reversal symmetry is broken and a gap is opened at the Dirac point. Magnetic TIs exhibit the quantum anomalous Hall effect (QAHE), where the longitudinal resistance drops to zero as the Hall resistance approaches the conductance quantum [6]. This dissipation-less longitudinal resistance both at zero field and high field is significant for potential zero-loss devices [7].

At present this phenomenon has only been observed at low temperature, primarily in magnetically doped TIs. The QAHE was first observed in Cr-doped $(\text{Bi,Sb})_2\text{Te}_3$ at 30 mK, and has since been seen in magnetically-doped TIs like Cr- or V-doped $(\text{Bi,Sb})_2\text{Te}_3$ at temperatures up to 2 K [8–10]. The inherent gap inhomogeneity induced by magnetic doping is believed to suppress the temper-

ature at which the QAHE is observed. Therefore, to observe the QAHE at higher temperatures, many have tried to induce a magnetic proximity effect in TIs with an adjacent ferromagnet.

The QAHE has been observed in one magnetic insulator/topological insulator heterostructure thus far: a $\text{Zn}_{1-x}\text{Cr}_x\text{Te}$ (ZCT)/ $(\text{Bi}_{1-y}\text{Sb}_y)_2\text{Te}_3$ (BST)/ZCT stack at 30 mK [11]. Common techniques used to confirm the magnetic proximity effect in the absence of observing the QAHE include Hall effect and polarized neutron reflectometry (PNR) measurements. In Hall effect measurements, an anomalous Hall resistance associated with spontaneous magnetization has been seen in a number of ferromagnetic insulator/TI layers for ferromagnets with both in-plane and out-of plane anisotropy, including $\text{Cr}_2\text{Ge}_2\text{Te}_6/\text{TI}$, $\text{Y}_3\text{Fe}_5\text{O}_{12}/\text{TI}$, $\text{Tm}_3\text{Fe}_5\text{O}_{12}/\text{TI}$, and LaCoO_3/TI bilayers [12–17]. Others have used PNR to detect magnetism induced in the TI layer in systems such as $\text{EuS}/\text{Bi}_2\text{Se}_3$ [18, 19]. However, in all these FI/TI heterostructures, there has yet to be definitive evidence of the QAHE at elevated temperatures.

In this letter, we have synthesized thin film bilayers of $\text{MgAl}_{0.5}\text{Fe}_{1.5}\text{O}_4$, a magnetic insulator, with Bi_2Se_3 to understand electrical transport measurements and polarized neutron reflectometry in the context of a MPE in Bi_2Se_3 . In addition, we use local structural characterization to obtain a complete description of the system. Nonlinear Hall effect data can be interpreted as signatures of an anomalous Hall effect or conduction of multiple carrier types. Magnetic profiles deduced from PNR data are consistent with either a MPE induced in Bi_2Se_3 or a disordered layer at the interface. However, x-ray reflectivity and transmission electron microscopy indicate an interfacial layer between the FI and TI consistent with interdiffusion at the interface rather than a MPE in the Bi_2Se_3 . Together, our results indicate that careful char-

acterization of microstructure is essential in identifying a magnetic proximity effect in a topological insulator.

13 nm of $\text{MgAl}_{0.5}\text{Fe}_{1.5}\text{O}_4$ (MAFO) was grown on as-received (001) oriented MgAl_2O_4 (MAO) single crystal substrates via pulsed laser deposition. Deposition details can be found in previous work [20, 21]. Subsequently, Bi_2Se_3 was deposited after *ex situ* transfer to an MBE chamber. The Bi_2Se_3 thickness was fixed at 8 nm, a thickness which exhibits strong characteristics of surface states but is sufficiently thin that the bulk states do not overwhelm electrical measurements. Details of growth can be found in the Supplement [22].

Electrical transport measurements were carried out to explore signatures of a magnetic proximity effect in these bilayers. We confirmed all electrical current was flowing through the Bi_2Se_3 layer by measuring the temperature dependent resistivity of the bilayer, which follows the expected temperature dependence for Bi_2Se_3 (seen in the Supplement [22]). We performed Hall effect measurements at a variety of temperatures. In general, a Hall effect signal is comprised of contributions from the ordinary Hall effect (OHE) due to the deflection of charge carriers by the Lorentz force as well as the anomalous Hall effect (AHE), which can have intrinsic and extrinsic origins [23]. The OHE leads to a Hall resistance proportional to the concentration of electronic carriers that may come from multiple bands. Materials with long range magnetic order exhibit an AHE that is attributed to the spontaneous magnetization and can be understood in terms of intrinsic and extrinsic (side-jump and skew scattering) factors.

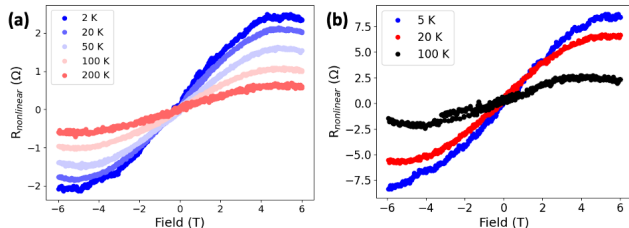


FIG. 1. Nonlinear Hall signal that remains after high field linear background subtraction for (a) a MAFO/ Bi_2Se_3 bilayer and (b) Bi_2Se_3 on an MAO substrate.

The Hall data initially looks linear [22]. We would expect any anomalous Hall resistance to be quite small compared to the ordinary Hall resistance, since the Bi_2Se_3 Fermi energy is far away from the Dirac point [24]. To separate the possible contributions to the Hall effect signal, we fit the high field Hall data (6 T - 8 T) to a line, corresponding to the ordinary Hall resistance. This linear fit is subtracted out of the data (see Supplement for details [22]). The remaining signal shows a large nonlinear contribution as a function of magnetic field. This signal, seen in Fig. 1(a), is around 2.5 Ω at 2 K and decreases monotonically with increasing temperature. We

consider two possible origins of this nonlinear signal- the AHE due to induced magnetism in the Bi_2Se_3 or a carrier from a second band contributing to the OHE. To determine whether this nonlinear behavior can be attributed to the Bi_2Se_3 film itself or a MPE, we performed Hall effect measurements on an 8 nm Bi_2Se_3 film grown on an MgAl_2O_4 substrate. The Bi_2Se_3 film in the control sample has the same lattice parameter as the Bi_2Se_3 layer in the bilayer sample since MAFO is coherently strained to MAO. Therefore the Bi_2Se_3 layers in both samples have qualitatively the same structure.

In the control Bi_2Se_3 /MAO sample, we find the same nonlinearity in the Hall effect with a slightly higher resistance (7.5 Ω) as seen in Fig. 1(b). This difference in magnitude is attributed to typical sample to sample variation in Bi_2Se_3 carrier concentration. We fit the data from the control sample to a two-carrier model (Eq. 1 in [22]). While this model is not well constrained, the fit estimates $n_1 \approx 2.4 \times 10^{13} \text{ cm}^{-2}$, $n_2 \approx 1.3 \times 10^{12} \text{ cm}^{-2}$, $\mu_1 \approx 700 \text{ cm}^2/\text{Vs}$, and $\mu_2 \approx 1600 \text{ cm}^2/\text{Vs}$. These values are similar to what has been reported in other studies of Bi_2Se_3 on a variety of substrates (Si, CdS, and Al_2O_3) and is attributed in these studies to the coexistence of carriers from surface conduction and carriers from bulk conduction [25–29]. However, it is possible this nonlinearity results from charge transfer or band bending at the spinel/ Bi_2Se_3 interface. Due to the variation in carrier concentration from sample to sample, it is not feasible to subtract out the contribution from multiple carriers in the Hall effect signal coming solely from the Bi_2Se_3 to see if there is an induced anomalous Hall contribution in bilayer samples. Additionally, since the MAFO magnetization does not show hysteresis in an out-of-plane field, we cannot definitively confirm that there is any MPE in the Hall effect measurements of bilayer samples.

Because electrical transport results were inconclusive, we employed polarized neutron reflectometry to directly probe the magnetic depth profile of our bilayer system. PNR has recently been extensively employed in the detection of magnetic proximity effects in topological insulators. Measurements were performed at 5 K in a 3 T in-plane magnetic field using the PBR instrument at the NIST Center for Neutron Research (see Supplement for experimental details [22]). The spin asymmetry, given by the difference of the two non spin-flip reflectivities normalized by their sum, is plotted in Fig. 2(a) as a function of Q , the momentum transfer along the film normal direction. The resulting nuclear and magnetic SLD density depth profiles found from fitting the spin-dependent specular reflectivities are shown in Fig. 2(b-c).

As with most PNR studies of magnetic proximity effects, the signal associated with induced magnetization in the Bi_2Se_3 layer is expected to be subtle while the MAFO magnetism will dominate the reflectivity features. Fitting the data for this heterostructure is consequently nontrivial, as slight changes in the MAFO magnetism or

structural differences at various film interfaces may imply different magnetic structures. Using a model with a MAFO profile very similar to that found in previous PNR studies of MAFO/MAO films, we see that a fit with a substantial MPE in the Bi_2Se_3 (profile in Fig. 2(b)) agrees with the data extremely well ($\chi^2 = 2.41$, the red line in Fig. 2(a))[30]. The result of refining a model with identical constraints except with no magnetism in the Bi_2Se_3 is shown with the blue line in Fig. 2(a). One can see such a fit does not capture all the features in the spin asymmetry, particularly the shoulder in the data around $Q=0.3 \text{ nm}^{-1}$, with a slight phase shift introduced into the spin asymmetry in the model where Bi_2Se_3 magnetization is forced to zero.

Despite the apparently strong evidence for a magnetic

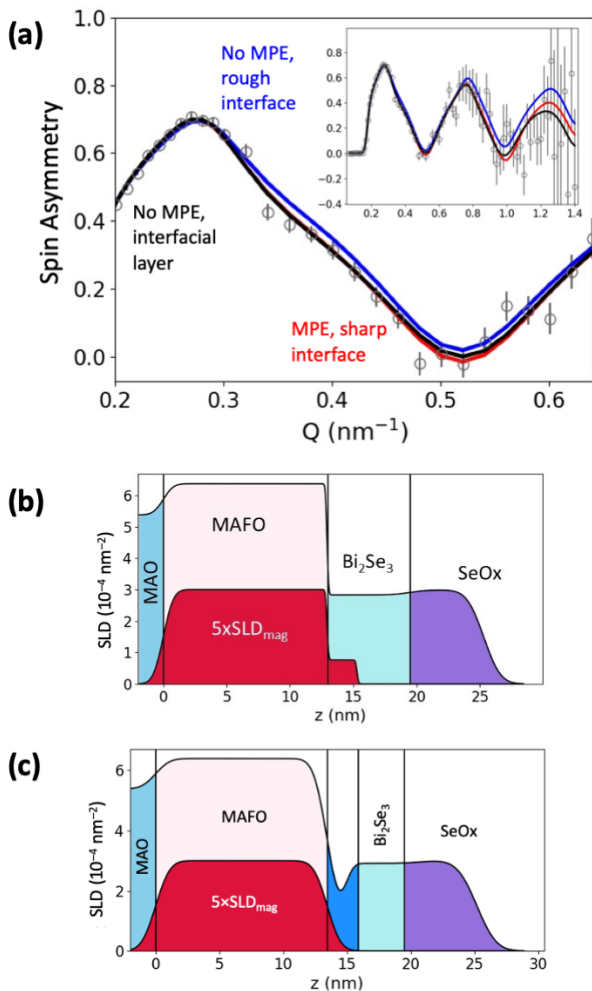


FIG. 2. PNR of 13 nm MAFO/8 nm Bi_2Se_3 bilayer. (a) Spin asymmetry (inset: full dataset). Error bars represent ± 1 standard deviation. (b) Profile with MPE in TI, no interfacial layer. (c) Profile with interfacial layer. By fitting the spin asymmetry in (a), the depth profile of the heterostructure can be modeled in (b) and (c).

proximity effect, we also investigated alternative explanations for the measured magnetic depth profile and considered three total models: one with a sharp MAFO/ Bi_2Se_3 interface, one with a rough interface, and one with a transitional growth region [22]. By broadening the constraints for MAFO/ Bi_2Se_3 interface quality to allow for a transitional growth region of lower Bi_2Se_3 density, we find an equally good fit ($\chi^2 = 2.48$, the black line in Fig. 2(a)) for the PNR data which predicts a low density interfacial layer between the MAFO and Bi_2Se_3 (Fig. 2(c)). In this model, the Bi_2Se_3 is restricted to have zero magnetization as in the previous comparative model. However, introduction of a transitional growth region allows the spin asymmetry features between 0.3 nm^{-1} and 0.5 nm^{-1} to be captured, eliminating the phase shift introduced by removing the Bi_2Se_3 interface magnetization. The coupling of magnetic and structural data in PNR allows for multiple interpretations, so further structural information is necessary to distinguish between them.

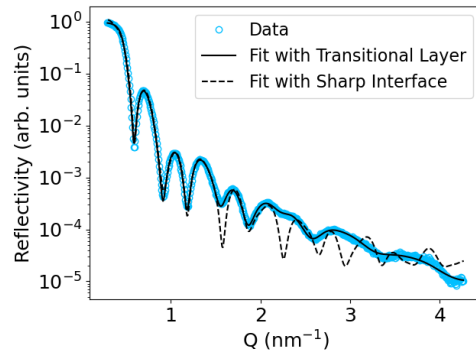


FIG. 3. X-ray reflectivity of a MAFO/ Bi_2Se_3 bilayer. The solid line indicates the best fit including an interfacial layer between the two materials, while the dashed line shows the best fit assuming no interfacial layer.

To determine the correct PNR model, we performed x-ray reflectivity (XRR). Although XRR does not provide the magnetic information of PNR, the increased intensity of an x-ray source allows measurements to be performed over a much larger Q -range (4 nm^{-1} vs. 1.4 nm^{-1}). Thin interface structures may consequently be much more finely resolved, allowing us to distinguish between candidate PNR models. Indeed, fitting the XRR data (seen in Fig. 3) reveals a low density interfacial layer between MAFO and Bi_2Se_3 ($\chi^2 = 7.96$). Attempting to fit the XRR data without an interfacial layer leads to a poor fit with $\chi^2 = 147.7$, shown with a dashed line in Fig. 3.

The presence of a low density layer is also consistent with annular dark-field scanning transmission electron microscopy (ADF-STEM) imaging and elemental analysis performed on the MAFO/ Bi_2Se_3 bilayers. We observe an interfacial layer which is partially crystalline, with sections of quintuple layers and other sections of

amorphous Bi and Se, seen in Fig. 4(a). Energy dispersive x-ray (EDX) maps provide the atomic percentage of each element as a function of depth, summarized in Fig. 4(b). We note there is a slight Bi excess seen in the Bi_2Se_3 layer, which has been seen in TEM studies of Bi_2Se_3 films before and may be due to signal interference of Bi and Se. Additionally, the Al and Se peaks are overlapping, so the Al signal is artificially high in the Bi_2Se_3 layer. From the EDX maps, we see that the disordered interfacial layer between the highly crystalline MAFO and Bi_2Se_3 has some compositional intermixing between the two materials.

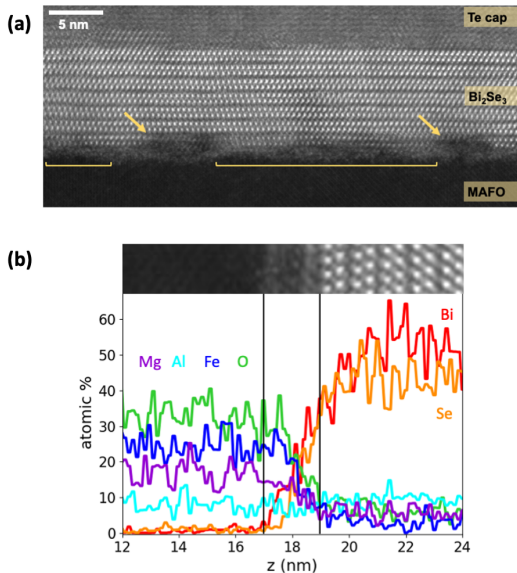


FIG. 4. (a) ADF-STEM image showing disorder at the MAFO/TI interface. Brackets and arrows indicate disordered interfacial regions with height of ~ 1 nm and ~ 2 nm, respectively. (b) EDX elemental analysis, showing an image of the region analyzed and an elemental line profile.

By observing the microstructure of the MI/TI bilayers, we can distinguish the PNR model that captures all the features of the spin asymmetry and is consistent with structural data. The low density layer between MAFO and Bi_2Se_3 we observe in XRR and TEM matches with the PNR model which does not provide any evidence of a MPE. Additionally, by comparing the bilayer Hall effect measurements with those of the control sample, we find it likely that the nonlinear Hall effect is due to multiple carriers in the TI rather than an AHE from a MPE in Bi_2Se_3 due to the adjacent MAFO.

Several studies perform Hall effect measurements and observe a nonlinear or even hysteretic contribution they attribute to an anomalous Hall effect. YIG, another commonly used magnetic insulator, has a lower saturation field than MAFO out of plane, so one may expect multiple carriers to not be an issue, as nonlinearity in the Hall effect due to contributions from multiple carriers is typi-

cally thought of as relevant over the field scale of several Tesla. However, this effect contributes at low field as well. When we take the two-carrier fit from the Bi_2Se_3 /MAO Hall data at 5 K and carry out the same background subtraction method, but only for ± 0.5 T, the resulting signal is still nonlinear with a magnitude of ~ 10 m Ω [22]. This is on the order of magnitude of other anomalous Hall signals in literature, which means this contribution is a major concern for all field values [16, 17, 31].

A handful of studies have investigated the microstructure of magnetic insulator/TI bilayers through TEM in addition to Hall effect or PNR measurements, showing high quality interfaces [11, 13]. However, not all provide conclusive evidence of a high quality interface [19, 32, 33]. For example, one study showed TEM of YIG/ Bi_2Te_3 with an apparently sharp interface [34]. Meanwhile, a structural study of YIG/ Bi_2Se_3 through TEM showed structural disorder in the TI layer with an amorphous interface, and another paper showed TEM with a clear interfacial layer [35–37]. PNR of MI/TI bilayers in a study of $\text{EuS}/\text{Bi}_2\text{Se}_3$ is used to demonstrate evidence of a magnetic proximity effect induced in the Bi_2Se_3 , and TEM is shown [18]. However, compositional data is not shown for the TEM, and only PNR models with a sharp structural interface between the two layers are explored. Recently, XMCD was performed on EuS/BST bilayers, and no magnetism was detected in the BST layer, contradicting this PNR study as well as studies which show an anomalous Hall effect [38]. Our work provides a lens through which to understand these contradictory results.

Our results point to the necessary conditions to claim a MPE in a magnetic insulator/topological insulator system. Multi-pronged approaches are imperative: one must couple structural data from TEM and XRR to any magnetic profiling done with PNR or other techniques. A sharp interface between materials must be established to avoid measuring signals from a rough interface or compositionally intermixed layer [39]. Moving forward, a combination of depth-resolved techniques like PNR with element-specific techniques like x-ray magnetic dichroism (XMCD) or resonant x-ray magnetic reflectivity (XRMR) would be ideal to establish magnetism in the TI [40–43]. Finally, transport signatures of a MPE are vital to measure if one wants to ultimately realize the QAHE. Only magnetic insulators with perpendicular magnetic anisotropy (PMA) should be considered suitable to induce a MPE in TIs, since any AHE contribution from a MI with in-plane anisotropy cannot be convincingly disentangled from multiple bands of carriers in the TI. A thorough temperature dependence of the anomalous Hall magnitude should be recorded to rule out any spin Hall effect contribution [44, 45].

Creating MI/TI heterostructures with a high-quality interface is a big challenge, but there are several possible solutions. First, *in situ* heterostructure growth with all-chalcogenide films have shown atomically sharp inter-

faces, due to matching crystal structures and avoiding hydrocarbon contamination [11, 46]. *Ex situ* growth can be successful with magnetic films which are robust to high temperature annealing and can grow epitaxially on standard substrates for TIs like Al_2O_3 [47]. In the absence of these options, exfoliating and transferring thin films of TIs may be preferable to attempting direct growth for a high-quality interface [48]. Notably, the sole observation of a proximity induced QAHE was in an *in situ* grown trilayer where an atomically sharp interface was verified with TEM [11].

We have performed comprehensive magnetic and structural characterization on thin film heterostructures of MAFO and Bi_2Se_3 to detect whether a magnetic proximity effect is induced in a topological insulator. We find two promising indications of magnetism induced in Bi_2Se_3 : a large nonlinear Hall effect that increases with decreasing temperature and polarized neutron reflectometry suggesting additional magnetism outside the MAFO layer. However, we find alternative ways to interpret the Hall and PNR data. In this system, structural data points to a disordered interfacial layer between the magnet and TI rather than a MPE in the TI. Our results suggest the importance of careful structural information in accurately detecting a magnetic proximity effect in the absence of observing the QAHE. Further, our work provides a framework of materials considerations to synthesize a high-quality heterostructure and experiments needed to identify a MPE.

This work at Stanford is supported by the Air Force Office of Scientific Research, Grant #FA9550-20-1-0293. LR is supported by an NSF graduate research fellowship. Part of this work was performed at the Stanford Nano Shared Facilities (SNSF), supported by the National Science Foundation under award ECCS-1542152. We acknowledge the financial support of the National Science Foundation through the Penn State 2D Crystal Consortium Materials Innovation Platform (2DCCMIP) under NSF cooperative agreement DMR1539916. D.R.H. and N.A. acknowledge support from the NSF CAREER program (DMR-1654107). This work utilized resources provided by the NSF-MRSEC-sponsored Materials Characterization Lab at Penn State (DMR-1420620). Certain trade names and company products are mentioned in the text or identified in an illustration in order to adequately specify the experimental procedure and equipment used. In no case does such identification imply recommendation or endorsement by the National Institute of Standards and Technology, nor does it imply that the products are necessarily the best available for the purpose.

* lridd@stanford.edu

[1] S.-Y. Huang, X. Fan, D. Qu, Y. P. Chen, W. G. Wang,

- J. Wu, T. Y. Chen, J. Q. Xiao, and C. L. Chien, *Physical review letters* **109**, 107204 (2012).
- [2] D. Zhong, K. L. Seyler, X. Linpeng, N. P. Wilson, T. Taniguchi, K. Watanabe, M. A. McGuire, K.-M. C. Fu, D. Xiao, W. Yao, *et al.*, *Nature nanotechnology* **15**, 187 (2020).
- [3] S. Bhattacharyya, G. Akhgar, M. Gebert, J. Karel, M. T. Edmonds, and M. S. Fuhrer, *Advanced Materials* **33**, 2007795 (2021).
- [4] M. Kiwi, *MRS Online Proceedings Library* **746**, 1 (2002).
- [5] Y. Tokura, K. Yasuda, and A. Tsukazaki, *Nature Reviews Physics* **1**, 126 (2019).
- [6] H. Ke, M. Xu-Cun, C. Xi, L. Li, W. Ya-Yu, and X. Qi-Kun, *Chinese Physics B* **22**, 067305 (2013).
- [7] M. Nadeem, A. R. Hamilton, M. S. Fuhrer, and X. Wang, *Small* **16**, 1904322 (2020).
- [8] C.-Z. Chang, J. Zhang, X. Feng, J. Shen, Z. Zhang, M. Guo, K. Li, Y. Ou, P. Wei, L.-L. Wang, *et al.*, *Science* **340**, 167 (2013).
- [9] J. G. Checkelsky, R. Yoshimi, A. Tsukazaki, K. S. Takahashi, Y. Kozuka, J. Falson, M. Kawasaki, and Y. Tokura, *Nature Physics* **10**, 731 (2014).
- [10] M. Mogi, R. Yoshimi, A. Tsukazaki, K. Yasuda, Y. Kozuka, K. Takahashi, M. Kawasaki, and Y. Tokura, *Applied Physics Letters* **107**, 182401 (2015).
- [11] R. Watanabe, R. Yoshimi, M. Kawamura, M. Mogi, A. Tsukazaki, X. Z. Yu, K. Nakajima, K. S. Takahashi, M. Kawasaki, and Y. Tokura, *Applied Physics Letters* **115** (2019), 10.1063/1.5111891, arXiv:1908.07163.
- [12] L. Alegria, H. Ji, N. Yao, J. Clarke, R. J. Cava, and J. R. Petta, *Applied Physics Letters* **105**, 053512 (2014).
- [13] M. Mogi, T. Nakajima, V. Ukleev, A. Tsukazaki, R. Yoshimi, M. Kawamura, K. S. Takahashi, T. Hanashima, K. Kakurai, T.-h. Arima, *et al.*, *Physical review letters* **123**, 016804 (2019).
- [14] Z. Jiang, C.-Z. Chang, C. Tang, P. Wei, J. S. Moodera, and J. Shi, *Nano letters* **15**, 5835 (2015).
- [15] C. Tang, C.-Z. Chang, G. Zhao, Y. Liu, Z. Jiang, C.-X. Liu, M. R. McCartney, D. J. Smith, T. Chen, J. S. Moodera, *et al.*, *Science advances* **3**, e1700307 (2017).
- [16] S. Zhu, D. Meng, G. Liang, G. Shi, P. Zhao, P. Cheng, Y. Li, X. Zhai, Y. Lu, L. Chen, *et al.*, *Nanoscale* **10**, 10041 (2018).
- [17] P. Wei, F. Katmis, B. A. Assaf, H. Steinberg, P. Jarillo-Herrero, D. Heiman, and J. S. Moodera, *Physical review letters* **110**, 186807 (2013).
- [18] F. Katmis, V. Lauter, F. S. Nogueira, B. A. Assaf, M. E. Jamer, P. Wei, B. Satpati, J. W. Freeland, I. Eremin, D. Heiman, P. Jarillo-Herrero, and J. S. Moodera, *Nature* **533**, 513 (2016).
- [19] M. Li, Q. Song, W. Zhao, J. A. Garlow, T.-H. Liu, L. Wu, Y. Zhu, J. S. Moodera, M. H. Chan, G. Chen, *et al.*, *Physical Review B* **96**, 201301(R) (2017).
- [20] S. Emori, D. Yi, S. Crossley, J. J. Wissner, P. P. Balakrishnan, B. Khodadadi, P. Shafer, C. Klewe, A. T. NDiaye, B. T. Urwin, *et al.*, *Nano letters* **18**, 4273 (2018).
- [21] L. J. Riddiford, J. J. Wissner, S. Emori, P. Li, D. Roy, E. Cogulu, O. van't Erve, Y. Deng, S. X. Wang, B. T. Jonker, *et al.*, *Applied Physics Letters* **115**, 122401 (2019).
- [22] "See supplemental material for additional details on thin film growth, characterization, and fitting of transport and polarized neutron reflectometry data, which includes refs. [49–51].".

- [23] N. Nagaosa, J. Sinova, S. Onoda, A. H. MacDonald, and N. P. Ong, *Reviews of modern physics* **82**, 1539 (2010).
- [24] Y. Xia, D. Qian, D. Hsieh, L. Wray, A. Pal, H. Lin, A. Bansil, D. Grauer, Y. S. Hor, R. J. Cava, *et al.*, *Nature physics* **5**, 398 (2009).
- [25] M. Brahlek, Y. S. Kim, N. Bansal, E. Edrey, and S. Oh, *Applied Physics Letters* **99**, 012109 (2011).
- [26] N. Bansal, Y. S. Kim, M. Brahlek, E. Edrey, and S. Oh, *Physical review letters* **109**, 116804 (2012).
- [27] L. He, F. Xiu, X. Yu, M. Teague, W. Jiang, Y. Fan, X. Kou, M. Lang, Y. Wang, G. Huang, *et al.*, *Nano letters* **12**, 1486 (2012).
- [28] A. A. Taskin, S. Sasaki, K. Segawa, and Y. Ando, *Physical review letters* **109**, 066803 (2012).
- [29] Z. Jiang, F. Katmis, C. Tang, P. Wei, J. S. Moodera, and J. Shi, *Applied Physics Letters* **104**, 222409 (2014).
- [30] J. J. Wisser, S. Emori, L. Riddiford, A. Altman, P. Li, K. Mahalingam, B. T. Urwin, B. M. Howe, M. R. Page, A. J. Grutter, *et al.*, *Applied Physics Letters* **115**, 132404 (2019).
- [31] Z. Jiang, C.-Z. Chang, C. Tang, P. Wei, J. S. Moodera, and J. Shi, *Nano Lett* **15**, 5840 (2015).
- [32] W. Yang, S. Yang, Q. Zhang, Y. Xu, S. Shen, J. Liao, J. Teng, C. Nan, L. Gu, Y. Sun, K. Wu, and Y. Li, *Applied Physics Letters* **105**, 092411 (2014).
- [33] A. Kandala, A. Richardella, D. Rench, D. Zhang, T. Flanagan, and N. Samarth, *Applied Physics Letters* **103**, 202409 (2013).
- [34] M. Lang, M. Montazeri, M. C. Onbasli, X. Kou, Y. Fan, P. Upadhyaya, K. Yao, F. Liu, Y. Jiang, W. Jiang, K. L. Wong, G. Yu, J. Tang, T. Nie, L. He, R. N. Schwartz, Y. Wang, C. A. Ross, and K. L. Wang, *Nano Lett* **14**, 3459 (2014).
- [35] D. Reifsnnyder Hickey, J. G. Azadani, A. R. Richardella, J. C. Kally, J. S. Lee, H. Chang, T. Liu, M. Wu, N. Samarth, T. Low, *et al.*, *Physical Review Materials* **3**, 061201(R) (2019).
- [36] D. Reifsnnyder Hickey and K. A. Mkhoyan, *APL Materials* **8**, 070902 (2020).
- [37] Z. Jiang, C.-Z. Chang, C. Tang, J.-G. Zheng, J. S. Moodera, and J. Shi, *AIP Advances* **6**, 055809 (2016).
- [38] A. I. Figueroa, F. Bonell, M. G. Cuxart, M. Valvidares, P. Gargiani, G. van der Laan, A. Mugarza, and S. O. Valenzuela, *Physical Review Letters* **125**, 226801 (2020).
- [39] S. Geprägs, C. Klewe, S. Meyer, D. Graulich, F. Schade, M. Schneider, S. Francoual, S. P. Collins, K. Ollefs, F. Wilhelm, *et al.*, *Physical Review B* **102**, 214438 (2020).
- [40] C.-Y. Yang, L. Pan, A. J. Grutter, H. Wang, X. Che, Q. L. He, Y. Wu, D. A. Gilbert, P. Shafer, E. Arenholz, *et al.*, *Science advances* **6**, eaaz8463 (2020).
- [41] C.-Y. Yang, Y.-H. Lee, K.-H. Ou Yang, K.-C. Chiu, C. Tang, Y. Liu, Y.-F. Zhao, C.-Z. Chang, F.-H. Chang, H.-J. Lin, *et al.*, *Applied Physics Letters* **114**, 082403 (2019).
- [42] T. Kuschel, C. Klewe, J.-M. Schmalhorst, F. Bertram, O. Kuschel, T. Schemme, J. Wollschläger, S. Francoual, J. Strempler, A. Gupta, *et al.*, *Physical review letters* **115**, 097401 (2015).
- [43] C. Klewe, T. Kuschel, J.-M. Schmalhorst, F. Bertram, O. Kuschel, J. Wollschläger, J. Strempler, M. Meinert, and G. Reiss, *Physical Review B* **93**, 214440 (2016).
- [44] Q. Shao, A. Grutter, Y. Liu, G. Yu, C.-Y. Yang, D. A. Gilbert, E. Arenholz, P. Shafer, X. Che, C. Tang, *et al.*, *Physical Review B* **99**, 104401 (2019).
- [45] S. Ding, Z. Liang, C. Yun, R. Wu, M. Xue, Z. Lin, A. Ross, S. Becker, W. Yang, X. Ma, *et al.*, *Physical Review B* **104**, 224410 (2021).
- [46] J. J. Bauer, P. Quarterman, A. J. Grutter, B. Khurana, S. Kundu, K. A. Mkhoyan, J. A. Borchers, and C. A. Ross, *Physical Review B* **104**, 094403 (2021).
- [47] L. Pan, A. Grutter, P. Zhang, X. Che, T. Nozaki, A. Stern, M. Street, B. Zhang, B. Casas, Q. L. He, *et al.*, *Advanced Materials* **32**, 2001460 (2020).
- [48] X. Che, K. Murata, L. Pan, Q. L. He, G. Yu, Q. Shao, G. Yin, P. Deng, Y. Fan, B. Ma, *et al.*, *ACS nano* **12**, 5042 (2018).
- [49] L. He, F. Xiu, Y. Wang, A. V. Fedorov, G. Huang, X. Kou, M. Lang, W. P. Beyermann, J. Zou, and K. L. Wang, *J. Appl. Phys* **109**, 103702 (2011).
- [50] B. Kirby, P. Kienzle, B. Maranville, N. Berk, J. Krycka, F. Heinrich, and C. Majkrzak, *Current Opinion in Colloid & Interface Science* **17**, 44 (2012).
- [51] B. Maranville, W. Ratcliff II, and P. Kienzle, *Journal of Applied Crystallography* **51**, 1500 (2018).